A continuous current model of fully-depleted symmetric double-gate MOSFETs considering a wide range of body doping concentrations

2010 Semicond. Sci. Technol. 25 055018

(http://iopscience.iop.org/0268-1242/25/5/055018)

Semicond. Sci. Technol. **25** (2010) 055018 (4pp) doi:10.1088/0268-1242/25/5/055018

A continuous current model of fully-depleted symmetric double-gate MOSFETs considering a wide range of body doping concentrations

Xiaoshi Jin[1], **Xi Liu**[1], **Jung-Hee Lee**[2] **and Jong-Ho Lee**[3]

[1] School of Information Science and Engineering, Shenyang University of Technology, Shenyang, People's Republic of China
[2] School of EECS, Kyungpook National University, 1370 Sangyuk-Dong Buk-Gu, Daegu 702-701, Korea
[3] School of EECS Eng. and ISRC (Inter-University Semiconductor Research Center), Seoul National University, Shinlim-Dong, Kwanak-Gu, Seoul 151-742, Korea

E-mail: jhl@snu.ac.kr

Received 27 December 2009, in final form 14 March 2010
Published 20 April 2010
Online at stacks.iop.org/SST/25/055018

Abstract
A continuous current model of fully-depleted symmetric double-gate (DG) MOSFETs which can reflect a wide range (from intrinsic to heavy doping) of the body doping concentrations was developed based on an approximated analytic potential solution of Poisson's equation. The model was compared with the results of device simulation, and showed very good agreement in all operation regions such as subthreshold, turn-on, linear and saturation.

1. Introduction

Double-gate (DG) FETs have been considered as candidates for next generation logic devices and memory cells due to their better performance and better scalability than those of single-gate FETs. In order to gain a physical insight of DG FETs and provide a fundamental basis for circuit simulation software, an analytical (or a compact) model should be derived. Models for undoped channel DG FETs have been reported [1–6]. Continuous drain current models are very attractive [3]. The body doping (N_b) in multi-gate FETs (a sort of DG FETs) for the application of memory cells can be increased [7, 8]. Therefore, a new continuous current model needs to be developed to consider N_b from nearly intrinsic to high doping. A closed form model has been given in [9]. However, this model needs a fitting parameter which should satisfy an empirical expression. A model considering partially and fully depleted body has been given in [10] where models are quite complicated and the channel potential is not analytic. A model for short channel DG devices with various N_bs has been reported in [11] where some fitting parameters are needed and the channel potential is not continuous. If those models become simpler, then these models are more useful for readers. A model which can reflect the body doping on the threshold voltage and channel potential of symmetric DG MOSFETs has been reported [12]; however, a continuous current model has not been given. In this work, we focus on the modeling of channel potential and drain current in fully-depleted (FD) DG FETs because the fully depletion is imperative in DG devices to improve scalability and performance. By using a reasonable initial guess and an appropriate boundary condition, we derive continuous channel potential for Poisson's equation considering both N_b and electron concentration in long channel DG devices. The continuous drain current model is derived based on the potential model and is verified by comparing with simulation results using the SILVACO tool [13].

2. Device structure

Figure 1 shows the schematic cross-sectional view of a DG MOSFET and the coordinate system. The fin body can be doped from intrinsic to high doping concentration with p-type impurity. The source and drain were heavily doped with n-type impurity. t_{ox} is the thickness of the oxide layer and L_g represents the gate length. The channel width and body thickness are marked as W and t_b, respectively. Since it

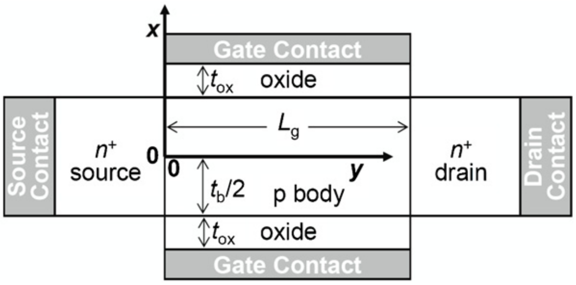

Figure 1. The schematic cross-sectional view of the DG MOSFET and the coordinate system. The gate length and body thickness are given by L_g and t_b, respectively.

is assumed that there are no oxide charges and no work-function difference between the gate and the body, the flat-band voltage (V_{fb}) is zero although the expression is given. A constant mobility of 200 cm^2 V^{-1} s^{-1} is used throughout this work.

3. Model and comparison with simulation results

According to the analysis of the quantum effect by numerical calculations [14], the classical model is basically valid for $t_b = 5$ nm. Therefore, in our derivation, we neglected the inversion layer quantum effect and use Poisson's equation to derive the expression of potential distribution. The parasitic source/drain series resistance was also not considered in our model.

Since the thin p-type body is fully depleted, the hole concentration in the body is also negligible. So we consider the acceptor concentration assuming that it is equal to N_b and the electron concentration in solving Poisson's equation as given in the following:

$$\nabla^2\psi(x) = \frac{q}{\varepsilon_{\rm si}}\left(N_b + n_i\,{\rm e}^{\frac{q(\psi-\psi_f)}{kT}}\right). \tag{1}$$

For the undoped case, the analytical solution has been given in [3]. To obtain analytic channel potential for various N_bs (from undoped to highly doped), a new approach is used as follows. In order to solve (1), we use the solution of the undoped case as an initial guess. The solution is given by

$$\psi\,(x) = \psi_{\rm f} - \frac{2kT}{q}\ln\left[\frac{t_b}{2\beta}\sqrt{\frac{q^2n_i}{2\varepsilon_{\rm si}kT}}\cos\left(\frac{2\beta x}{t_b}\right)\right], \tag{2}$$

where β is an integral constant, $\varepsilon_{\rm si}$ is the permittivity of Si and ψ_f is the quasi-Fermi potential [3]. Substituting (2) back into Poisson's equation (1), we obtain the following expression:

$$\nabla^2\psi\,(x) = \frac{q}{\varepsilon_{\rm si}}\left[N_b + \frac{8\beta^2\varepsilon_{\rm si}kT}{t_b^2q^2}\sec^2\left(\frac{2\beta x}{t_b}\right)\right]. \tag{3}$$

Integrating (3) about x twice, the solution of (3) is given by

$$\psi(x) = \frac{q}{\varepsilon_{\rm si}}\left\{\frac{N_bx^2}{2} - \frac{2\varepsilon_{\rm si}kT}{q^2}\ln\left[\cos\left(\frac{2\beta x}{t_b}\right)\right]\right\} + C_1x + C_2, \tag{4}$$

where C_1 and C_2 are both integral constants. Due to symmetry, (4) should be an even function with x; then C_1 should be 0. Using the boundary condition ($\psi(x = \pm t_b/2) = \psi_s$) below

$$\psi_s = V_{gs} - V_{fb} + \frac{\varepsilon_{\rm si}\xi_s t_{\rm ox}}{\varepsilon_{\rm ox}}, \tag{5}$$

where ψ_s and ξ_s are the surface potential and electric field, respectively, we can obtain C_2 as follows:

$$C_2 = V_{gs} - V_{fb} - \frac{qN_bt_bt_{\rm ox}}{2\varepsilon_{\rm ox}} - \frac{4\beta\varepsilon_{\rm si}t_{\rm ox}kT}{t_bq\varepsilon_{\rm ox}}\tan(\beta) - \frac{qN_bt_b^2}{8\varepsilon_{\rm si}} + \frac{2kT}{q}\ln[\cos(\beta)]. \tag{6}$$

Finally the potential expression reflecting a wide range of N_b can be expressed as

$$\psi(x) = \frac{qN_b\left(4x^2 - t_b^2\right)}{8\varepsilon_{\rm si}} + \frac{2kT}{q} \times \left\{\ln\left[\cos\left(\beta\right)\right] - \ln\left[\cos\left(\frac{2\beta x}{t_b}\right)\right]\right\} + V_{gs} - V_{fb} - \frac{qN_bt_bt_{\rm ox}}{2\varepsilon_{\rm ox}} - \frac{4\beta\varepsilon_{\rm si}t_{\rm ox}kT}{t_bq\varepsilon_{\rm ox}}\tan\left(\beta\right). \tag{7}$$

From one-dimensional Gauss's law:

$$2\varepsilon_{si}\xi_s = Q_i + Q_d, \tag{8}$$

where

$$Q_d = qN_bt_b \tag{9}$$

is the depletion charge density. The inversion charge density Q_i can be calculated as

$$Q_i = 2qn_i\int_0^{t_b/2}{\rm e}^{\frac{q(\psi-\psi_f)}{kT}}\,{\rm d}x. \tag{10}$$

Substituting (9) and (10) into (8), the quasi-Fermi potential can be expressed as

$$\psi_f = -\frac{kT}{q}\ln\left[\frac{4\beta\varepsilon_{\rm si}kT\tan\left(\beta\right)}{t_bq^2n_i\int_0^{t_b/2}{\rm e}^{\frac{q\psi}{kT}}\,{\rm d}x}\right]. \tag{11}$$

This is the relationship between the quasi-Fermi potential and the integral constant β. From the source to drain, ψ_f shifts from 0 to V_{ds}. β_s and β_d correspond to the ψ_f s which are 0 and V_{ds} at the source and drain, respectively, and both of them are determined from (11). Finally, the current can be calculated as

$$I_d = \mu_n\frac{W}{L_g}\int_{\beta_s}^{\beta_d}{\rm d}\beta\frac{\partial\psi_f}{\partial\beta}\int_0^{t_b/2}2qn_i\,{\rm e}^{\frac{q(\psi-\psi_f)}{kT}}. \tag{12}$$

In figure 2, I_d–V_{gs} curves from our compact model are compared with those from numerical simulation results (open symbols) as a parameter of N_b. The model *I*–*V* curve (solid line) when N_b is undoped is plotted as a reference [3] and shows excellent agreement with simulation data represented by open rectangular symbols. Here, since we assumed that the work-function of the gate electrode is the same as that of the body, the gate has a mid-gap work-function for the intrinsic N_b. The model *I*–*V* curves when the body is doped are represented by other solid lines and match very well with the simulated

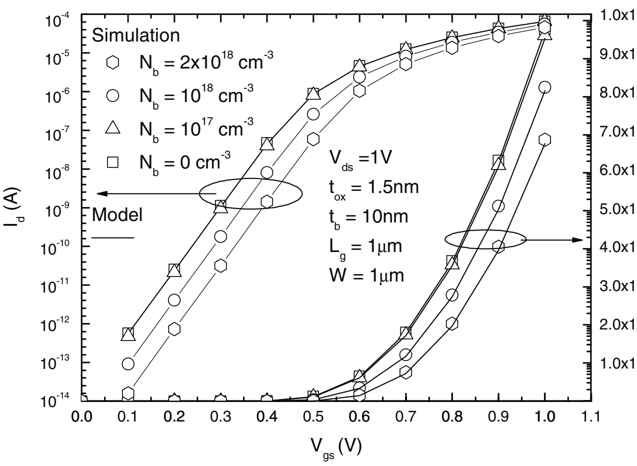

Figure 2. Comparison of I_d–V_{gs} curves between the compact model and simulation results with different body doping concentrations. The dotted line and solid lines represent the I_d–V_{gs} curves from the model when the body doping concentrations are intrinsic and doped, respectively. Simulation data are represented by open symbols. The same currents are plotted on both logarithmic (left) and linear (right) scales.

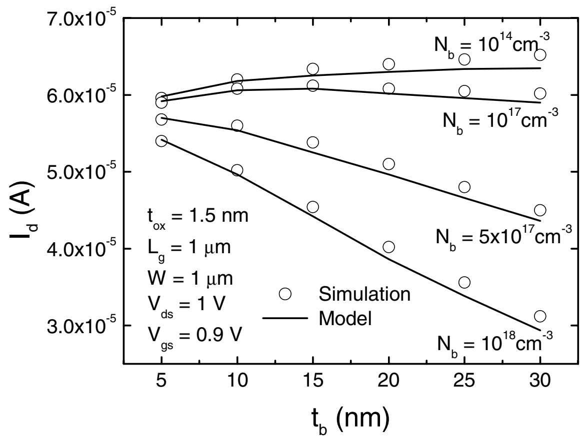

Figure 4. Comparison of I_d–t_b correlation between the model and simulation results with different body doping concentrations. V_{gs} is 0.9 V at a fixed V_{ds} of 1 V.

data represented by open symbols in all operation regions. For the N_bs less than 1×10^{17} cm^{-3}, N_b has no appreciable effect in threshold voltage. As shown in figure 2, our compact current model based on the analytical potential model explains very well the *I*–*V* behavior of DG devices with various N_bs from nearly undoped case to heavily doped case to 2×10^{18} cm^{-3}, which means our model clearly advances the model in [3].

Figure 3(*a*) shows the comparison of I_d–V_{ds} curves between the compact model and simulation results with different body doping concentrations when V_{gs} is 1 V and the t_b is 5 nm. The open symbols represent simulation data. Form this figure, we can clearly see that in both linear and saturation regions, the model gives very good agreement with simulation results. Also, we can see that even when the body doping concentration is increased to 5×10^{18} cm^{-3}, the accuracy of this model is maintained. Figure 3(*b*) shows the comparison of I_d–V_{ds} curves between the compact model and simulation results with different body thicknesses when V_{gs} is 1 V and N_b is 5×10^{18} cm^{-3}. The accuracy is maintained when the body thickness shifts from 30 nm to 5 nm.

Figure 4 shows the comparison of I_d–t_b correlation between the model and simulation results with different N_bs at a given V_{ds} of 1 V · V_{gs} is 0.9 V (turn-on). In general, heavier N_b gives smaller drain current at the same external biases. When N_b is heavy, increasing t_b increases the threshold voltage so that the drain current decreases. However, the drain current of the devices with lightly doped body increases with increasing t_b because the channel potential slightly increases under the same bias condition. In the case of moderate N_b, for example, $N_b = {\sim}10^{17}$ cm^{-3}, the current behavior with t_b is not monotonic. For the moderate channel doping, we can optimize t_b to maximize the current drivability.

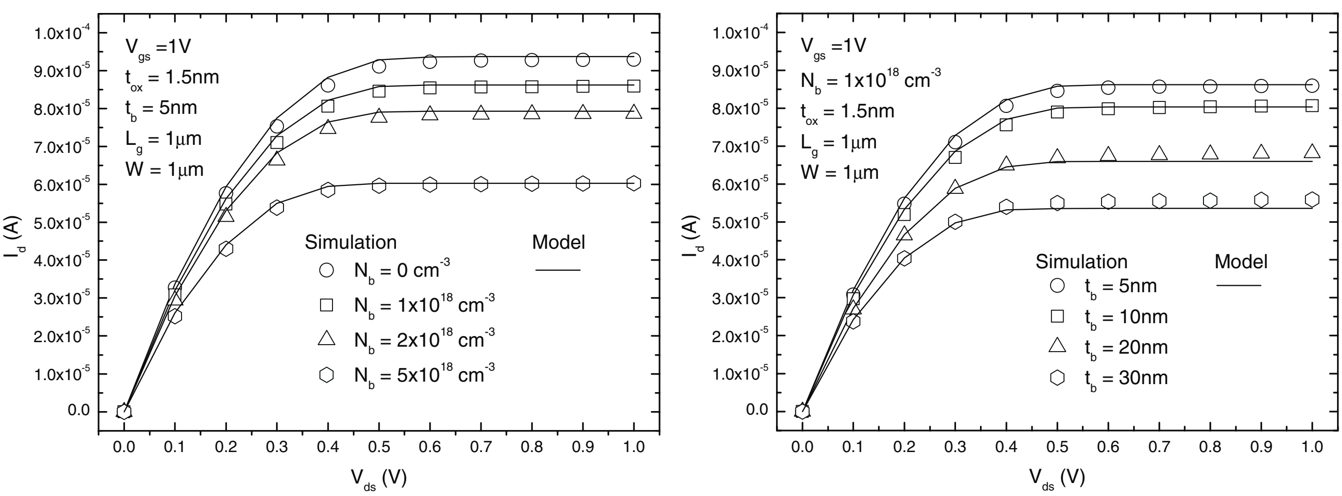

(*a*) (*b*)

Figure 3. Comparison of I_d–V_{ds} curves between the compact model and simulation results with different body thicknesses.

4. Conclusion

A continuous compact current model of fully-depleted symmetric DG MOSFETs with various body doping concentrations (from intrinsic to high doping) has been developed by solving Poisson's equation approximately. The total current model which consists of both drift and diffusion components was compared with simulation results and showed very good agreement in subthreshold, turn-on, linear and saturation regions at different body doping concentrations. We believe our model provides fundamentals in understanding fully-depleted DG devices with various body dopings and can be used in circuit simulation.

References

[1] Taur Y 2000 *IEEE Electron. Device Lett.* **21** 245–947
[2] Taur Y 2001 *IEEE Trans. Electron. Devices* **48** 2861–69
[3] Taur Y, Liang X, Wang W and Lu H 2004 *IEEE Electron. Device Lett.* **25** 107–9
[4] Lu H and Taur Y 2006 *IEEE Trans. Electron. Devices* **53** 1161–8
[5] Yu B, Lu H, Liu M and Taur Y 2007 *IEEE Trans. Electron. Devices* **54** 2715–22
[6] Lu H, Yu B and Taur Y 2008 *Solid-State Electron* **52** 67–72
[7] Park J M *et al* 2006 *IEDM Tech. Dig.* pp 1–4
[8] Park T S, Cho H J, Choe J D, Cho I H, Park D, Yoon E and Lee J H 2006 *IEEE Electron. Device Lett.* 889–92
[9] Lee M, Tang J, Lv Y and Yu Z 2009 *Chin. Phys. Lett.* **26** 018501
[10] Liu F, He J, Zhang J, Chen Y and Chan M 2008 *IEEE Trans. Electron. Devices* **55** 3494–502
[11] Cerdeira A, Iñiguez B and Estrada M 2008 *Solid-State Electron.* **52** 1064–70
[12] Liu F, Zhang L, Zhang J, He J and Chan M 2009 *Semicond. Sci. Technol.* **24** 085005
[13] SILVACO International 2005 ATLAS User's Manual
[14] Shoji M and Horiguchi S 1999 *J. Appl. Phys.* **85** 2722–31